A semi-empirical model to predict the EM38 electromagnetic induction measurements of soils from basic ground properties

FERNANDO VISCONTI*, JOSÉ MIGUEL DE PAZ

Instituto Valenciano de Investigaciones Agrarias–IVIA (GV), Centro para el Desarrollo de la Agricultura Sostenible–CDAS, Carretera CV-315, Km 10.7, 46113 Moncada, València, Spain.

***Corresponding Author:** Fernando Visconti. (E-mail: visconti_fer@gva.es).

Running Title: A model for electromagnetic induction measurements

Summary

Electromagnetic induction (EMI) measurements (σ_b*) are widely used for the survey of several soil attributes, among which basic properties such as salinity (σ_e), water content (θ_w), clay (w_c), organic matter (w_{om}) and bulk density (ρ_b) stand out. In the usual practice, purely empirical models relating one of these properties to σ_b* are calibrated in selected sites. However, this calibration is site and time specific and has to be repeated one time and again.

In order to understand where the variability of the EMI empirical models comes from, it is necessary to know how the different soil properties contribute to them and, for this aim, a more physically-based relationship between σ_b* and, at least, σ_e, θ_w, w_c, w_{om}, ρ_b was developed in this work, additionally including soil temperature (t). It was calibrated and cross-validated with the data from one survey done in a wide agricultural irrigation area in SE Spain taking σ_b* measurements with the Geonics EM38 in the horizontal and vertical dipole modes and at various heights over the ground. Then, it was externally validated with the data from a second survey carried out four years later in the same area but in a different season.

In the calibration R^2 was 0.84 and RMSE 0.18 dS/m (41%) for the vertical dipole orientation and 0.90 and 0.11 dS/m (39%) for the horizontal one. In the external validation, R^2 was 0.80 and RMSE 0.24 dS/m (44%) for the vertical dipole orientation and, respectively, 0.90 and 0.13 dS/m (38%) for the horizontal one.

Therefore, since the performance of the model barely worsened as time passed by, it can be considered to represent the underlying physical process and, therefore, to increase our understanding of how the soil EMI signals are generated with potential benefits for the planning and comparability of EMI soil measurements, specifically with the EM38, among different areas.

Keywords: salinity, water content, texture, organic matter, electromagnetic induction

Highlights:

A semi-empirical model was developed to predict soil EMI measurements from basic ground properties.

Salinity, water content, clay, organic matter, bulk density, and temperature were used as predictors.

The model was able to explain between 80 and 90% of the variance in EMI measurements in the validation.

This model helps us understand how the basic soil properties contribute to the EMI measurements.

Symbols and abbreviations:

A list has been provided as Supporting Information Material 1 (SIM 1)

Introduction

Soils conduct electricity since they contain ions, which act as charge carriers and, additionally, water, which acts as a transport medium. Conceptually, conduction in soil takes place in the liquid water that surrounds the soil solid particles by means of the ions moving through the soil pore water, and by the exchange ions moving along the solid-water interfaces (Jurinak et al., 1987; Kelleners et al., 2004). Therefore, the aggregated ability of a soil to conduct electricity, i.e., the soil bulk electrical conductivity (σ_b) depends on a) the salt, or ion, content, which is usually expressed as the electrical conductivity at 25 ºC of the saturation extract (σ_e), b) the volumetric water content (θ_w), c) the bulk density (ρ_b), d) the amount of exchange ions, which is generally equal to the cation exchange capacity (*CEC*), and e) temperature (t). Providing *CEC* essentially depends on the soil clay and organic matter fractions, σ_b can be considered to ultimately depend on the mineralogy and mass fractions of clay (w_c) and organic matter (w_{om}) in addition to σ_e, θ_w, ρ_b and t (McNeill, 1992; Rhoades et al., 1999).

Nowadays there are several electromagnetic techniques for σ_b sensing: electrical resistivity (ER), time domain reflectometry (TDR), frequency domain reflectometry (FDR) and electromagnetic induction (EMI) (Visconti & de Paz, 2016). Compared to ER, TDR and FDR, EMI presents one important advantage for data collection because it does not require soil contact. Therefore, since EMI instruments are non-invasive, they can be mounted on non-conductive custom-made vehicles, connected to data loggers and GPS navigation devices and towed along large expanses of lands for fast, frequent and cost-effective surveys (Carter et al., 1993; Sudduth et al., 2001; Triantafilis et al., 2002; Freeland et al., 2002).

EMI instruments are made up of at least two coils: one transmitter (Tx) that generates a primary time-varying magnetic field of H_p amplitude and one receiver (Rx) that responds to a secondary time-varying magnetic field of H_s amplitude generated at Rx by both the Tx and the soil (McNeill, 1980). The ratio of the quadrature component of H_s ($H_{s,\pi/2}$) to H_p depends on the σ_b and the soil magnetic permeability (μ), which can be considered equal to the vacuum permeability ($\mu_0 = 4\pi\ 10^{-7}$ H m^{-1}), and, additionally, on the primary field frequency (f) and the spacing between the Tx and Rx (r), their relative orientation (coplanar, crosswise, etc.) and, importantly, on the closeness and orientation of the whole EMI instrument to the soil (vertical, horizontal, etc.) (de Jong et al., 1979). Since the σ_b varies with depth, a depth-weighted average bulk electrical conductivity measurement represented by σ_b* and related to the previously-commented parameters by:

$$\sigma_b{}^* = \frac{4(H_{s,\pi/2}/H_p)}{\mu_0 \omega r^2} \qquad (1),$$

is taken in the Rx coil and presented to the user (McNeill, 1980). This σ_b* measurement ultimately depends on the same soil properties that σ_b, namely, σ_e, θ_w, w_c, w_{om}, ρ_b and t. Besides, several σ_b* measurements can be taken by changing the orientation and height over the ground of the EMI instrument. For example, the widely used EM38 (Geonics Ltd., Mississauga, Ontario, Canada) has only two parallel 1-m apart Tx and Rx coils (r = 1 m), and measurements are commonly taken in horizontal coplanar ($\sigma_{b(H)}$*) and vertical coplanar ($\sigma_{b(V)}$*) 'dipole' orientations and at different heights (h) over the ground from the surface to up to 2 m (Corwin & Rhoades, 1990) to give 2 m measurements: $\sigma_{b(Vhi)}$*,… $\sigma_{b(Vhm)}$*, $\sigma_{b(Hhi)}$*,… $\sigma_{b(Hhm)}$*. Then, the σ_b of as many as 2 m different soil layers can be assessed from the σ_b* measurements by means of an inverse matrix multiplication, i.e., a 1D inversion (Borchers et al., 1997; Hendrickx et al., 2002).

The composite nature of σ_b, and the even more complex σ_b*, complicates the use and interpretation of EMI measurements. Therefore, EMI instruments require calibration for the soil factor under study and recalibration as soon as the other soil factors on which conductivity depends significantly change in mean and/or range of variation along the lands (Corwin & Rhoades, 1990). Despite this inconvenience, EMI has been thoroughly used in soil studies, primarily for the appraisal and delineation of salinity, but also θ_w, textural class and w_c, ρ_b and, recently, even w_{om} (Table 1).

[Table 1]

The calibration of EMI instruments is usually carried out by means of ordinary least squares regression and multiple linear regression, but also by means of principal components regression (PCR), partial least squares regression (PLSR), geostatistical modelling and other related techniques (Lesch et al., 1995; Lesch et al., 2000; Triantafilis et al., 2000). These approaches have, however, one important drawback: statistical models are functional, i.e., they represent just the data generating process (Cox, 2006), thus giving poor insight into the underlying physical mechanisms. For σ_b, physically-based models have been developed for use along with ER (Rhoades et al., 1976; Kizito et al., 2008), TDR (Kelleners & Verma, 2010) and FDR techniques (Visconti et al., 2014). Nevertheless, a physically-based model of the form $\sigma_b^* = \sigma_b^*(\sigma_e, \theta_w, w_c, w_{om}, \rho_b, t)$ has never been developed to our best knowledge for use along with EMI instruments. The development of, at least, a semi-empirical model would increase our insight into the EMI signal physics. This will help the planning of EMI measurement campaigns and the interpretation of their results. This is of the utmost importance since EMI continues to be widely used for the survey of soil properties all around the World (Heil & Schmidhalter, 2017).

The objective of this investigation was to develop, including calibration and validation, a semi-empirical model to predict the measurements taken with an EMI device (σ_b*), specifically the EM38, using salinity along with the volumetric soil water content, the mass fractions of clay and organic matter, bulk density and, additionally, temperature, as predictors in order to understand how these properties contribute to form the EMI signal. This kind of study is absent in the literature and much needed.

Model theory and development

A model for σ_b* prediction on the basis of σ_e, θ_w, w_c, w_{om}, ρ_b and t was developed starting with the linear relationship (Eq. 2) between a set of σ_b* measurements taken with the EM38 in the vertical and horizontal dipole orientations at various heights (h) over the ground from h_1 to h_m ($\sigma_{b(Vh1)}$*, $\sigma_{b(Vh2)}$*,... $\sigma_{b(Vhm)}$*, $\sigma_{b(Hh1)}$*, $\sigma_{b(Hh2)}$*,... $\sigma_{b(Hhm)}$*) and the σ_b of the different layers in which the ground can be split from d_1 to d_n ($\sigma_{b(d1)}$, $\sigma_{b(d2)}$,… $\sigma_{b(dn)}$) (Borchers et al., 1997; Hendrickx et al., 2002):

$$\begin{bmatrix} \sigma_{b(Vh_1)}* \\ \sigma_{b(Vh_2)}* \\ \dots \\ \sigma_{b(Vh_m)}* \\ \sigma_{b(Hh_1)}* \\ \sigma_{b(Hh_2)}* \\ \dots \\ \sigma_{b(Hh_m)}* \end{bmatrix} = \begin{bmatrix} \int_0^{d_1} \varphi_V(z+h_1)dz & \int_{d_1}^{d_2} \varphi_V(z+h_1)dz & \dots & \int_{d_{n-1}}^{d_n} \varphi_V(z+h_1)dz \\ \int_0^{d_1} \varphi_V(z+h_2)dz & \int_{d1}^{d_2} \varphi_V(z+h_2)dz & \dots & \int_{d_{n-1}}^{d_n} \varphi_V(z+h_2)dz \\ \dots & \dots & \dots & \dots \\ \int_0^{d_1} \varphi_V(z+h_m)dz & \int_{d_1}^{d_2} \varphi_V(z+h_m)dz & \dots & \int_{d_{n-1}}^{d_n} \varphi_V(z+h_m)dz \\ \int_0^{d_1} \varphi_H(z+h_1)dz & \int_{d_1}^{d_2} \varphi_H(z+h_1)dz & \dots & \int_{d_{n-1}}^{d_n} \varphi_H(z+h_1)dz \\ \int_0^{d_1} \varphi_H(z+h_2)dz & \int_{d_1}^{d_2} \varphi_H(z+h_2)dz & \dots & \int_{d_{n-1}}^{d_n} \varphi_H(z+h_2)dz \\ \dots & \dots & \dots & \dots \\ \int_0^{d_1} \varphi_H(z+h_m)dz & \int_{d_1}^{d_2} \varphi_H(z+h_m)dz & \dots & \int_{d_{n-1}}^{d_n} \varphi_H(z+h_m)dz \end{bmatrix} \begin{bmatrix} \sigma_{b(d_1)} \\ \sigma_{b(d_2)} \\ \dots \\ \sigma_{b(d_n)} \end{bmatrix} \quad (2),$$

where z expresses the downward coordinate and the matrix coefficients express the integrated contribution of each soil layer to each sensor measurement according to the known sensitivity functions for the vertical and horizontal dipole measurement modes featuring the EM38 (McNeill, 1980):

$$\varphi_{\mathrm{V}}(z) = \frac{4z}{(4z^2+1)^{3/2}} \quad (3), \qquad \varphi_{\mathrm{H}}(z) = 2 - \frac{4z}{(4z^2+1)^{1/2}} \quad (4).$$

The linear model represented by Eq. 2, in addition to Eq. 3 and Eq. 4, is valid as long as the induction number (N_{B}) for the soil is low enough ($N_{\mathrm{B}} << 1$). The N_{B} is defined as the ratio of the intercoil separation (r) to the skin depth (δ) when the EMI instrument lays on the soil. The skin depth δ is the soil depth needed to decrease the amplitude of the primary magnetic field from H_{p} to $H_{\mathrm{p}}/\mathrm{e}$ ($\approx 0.368\ H_{\mathrm{p}}$) and depends on the angular frequency of the primary time-varying magnetic field ($\omega = 2\pi f$) and the σ_{b} of the soil ($\overline{\sigma_{\mathrm{b}}}$) through:

$$N_{\mathrm{B}} = \frac{r}{\delta} = r\sqrt{\frac{\mu_0 \omega \overline{\sigma_{\mathrm{b}}}}{2}} \quad (5).$$

Eq. 5 was originally posed for a homogeneously conductive soil, i.e., one with a σ_{b} constant from topsoil to subsoil and below (McNeill, 1980). However, since such a soil never exists, a depth-weighted average σ_{b}, i.e., $\overline{\sigma_{\mathrm{b}}}$, calculated according to Eq. 6 is used in this work for N_{B} evaluation, where Δd_j is the thickness of the jth soil layer:

$$\overline{\sigma_{\mathrm{b}}} = \frac{\sum_{j=1}^{n} \sigma_{\mathrm{b}(d_j)} \Delta d_j}{\sum_{j=1}^{n} \Delta d_j} \quad (6).$$

Once the hypothesis of $N_{\mathrm{B}} << 1$ can be assumed, Eq. 2 can be reliably used for the calculation of the σ_{b} of the several soil layers ($n \leq 2\ m$) in which the soil can be split from $j = 1$ to n ($\sigma_{\mathrm{b}(dj)}$). Therefore, each $\sigma_{\mathrm{b}(dj)}$ value in Eq. 2 can be related to the pore water electrical conductivity at the soil temperature when the measurement was taken ($\sigma_{\mathrm{p},t}$), the volumetric soil water content (θ_{w}), the bulk density (ρ_{b}) and the cation exchange capacity (*CEC*) of its corresponding soil layer by means of the following physically-based equation, whose derivation is shown in Kelleners and Verma (2010):

$$\sigma_{\mathrm{b}} = \theta_{\mathrm{w}} T \left[\sigma_{\mathrm{p},t} + \frac{\mathrm{B}\rho_{\mathrm{b}} CEC}{\theta_{\mathrm{w}}} \right] \quad (7),$$

where B is the equivalent conductance of the counterions on the exchange complex in units of dS m^2 mol$_\mathrm{C}^{-1}$ provided ρ_b is in g cm^{-3}, *CEC* in mmol$_\mathrm{C}$ kg^{-1} and σ_b in dS m^{-1}, and *T* is the tortuosity, structure or formation factor, which is related to the soil structure, i.e., the arrangement of the soil solid particles and the in-between air-filled and water-filled voids, and depends again on its volumetric soil water content and, in its simplest, takes the following linear formulation where a and b are two dimensionless parameters provided θ_w is dimensionless too (Rhoades et al., 1976):

$$T = \mathrm{a}\, \theta_{\mathrm{w}} + \mathrm{b} \quad (8).$$

The electrical conductivity of saline aqueous solutions, i.e., $\sigma_{\mathrm{p},t}$ in equation 7, is known to increase as temperature (*t*) does at a rate of roughly 2% per ºC, and this relationship can be modelled through an empirical equation like the following:

$$\sigma_{\mathrm{p},t} = \sigma_{\mathrm{p},25}/\mathrm{f}(t) \quad (9),$$

where $\sigma_{\mathrm{p},25}$ is the pore water electrical conductivity at 25 ºC and f(*t*) is a temperature function given by (Sheets & Hendrickx, 1995; Corwin & Lesch, 2005):

$$\mathrm{f}(t) = 0.4470 + 1.4034\mathrm{e}^{-t/26.815} \quad (10).$$

The $\sigma_{\mathrm{p},25}$ value can be related to the soil (soluble) salt content represented by the electrical conductivity at 25 ºC of the saturation extract of the corresponding layer (σ_e) through the following semi-empirical equation (Eq. 11):

$$\sigma_{\mathrm{p},25} = \sigma_{\mathrm{p0}} + \mathrm{k}_{\sigma} \frac{w_{\mathrm{e}}\sigma_{\mathrm{e}}}{w_{\mathrm{w}}} \quad (11),$$

where the factor $w_\mathrm{e}/w_\mathrm{w}$ is the concentration ratio from the mass fraction of water in the saturated paste (w_e), to the mass fraction of water in the field at the time of measurement (w_w), and where the factors σ_{p0} (in units of dS/m) and k_σ (dimensionless), are two empirical coefficients included to take account of various effects that make the relationship between σ_p and σ_e depart from the simple dilution ratio that is represented by $\sigma_{p,25} = w_e\, \sigma_e / w_w$. These effects are, mainly, the precipitation of the soil salts of limited solubility calcite and gypsum, the cation exchange dilution effect and the anion exclusion (Visconti & de Paz, 2012).

The w_e in Eq. 11 can be considered to linearly depend on the mass fraction of soil clay (w_c) through a simple pedotransfer function like the following:

$$w_e = \mathrm{w}_{e0} + \mathrm{k}_{c,e}\, w_c \qquad (12).$$

where the coefficients w_{e0} and $\mathrm{k}_{c,e}$ (both dimensionless) were obtained previously for the study area using simple linear regression (Visconti, 2009).

Besides, the field mass fraction of soil water in equation 7 can be calculated from θ_w, ρ_b and water density (ρ_w) through Eq. 13:

$$w_w = \theta_w\, \rho_w / \rho_b \qquad (13).$$

Finally, the *CEC* in Eq. 7 is known to essentially depend for most soils on the mass fractions of clay and organic matter (Bell & van Keulen, 1995; Krogh et al., 2000) through a pedotransfer function like the following:

$$CEC = \mathrm{CEC}_0 + \mathrm{k}_{c,CEC}\, w_c + \mathrm{k}_{om,CEC}\, w_{om} \qquad (14),$$

where w_{om} is the mass fraction of soil OM and the coefficients $\mathrm{k}_{c,CEC}$ and $\mathrm{k}_{om,CEC}$ were found for the study area using multiple linear regression (Visconti, 2009).

Equations 8 to 14 can be combined to obtain Eq. 15 in which σ_b depends only on σ_e, θ_w, w_c, w_{om}, ρ_b and t:

$$\sigma_b = (\mathrm{a}\theta_w + \mathrm{b})\left[\frac{\sigma_{p0}\theta_w}{\mathrm{f}(t)} + \mathrm{k}_\sigma \frac{\rho_b}{\rho_w}\frac{\sigma_e}{\mathrm{f}(t)}\left(\mathrm{w}_{e0} + \mathrm{k}_{c,e} w_c\right) + \mathrm{B}\rho_b\left(\mathrm{CEC}_0 + \mathrm{k}_{c,CEC} w_c + \mathrm{k}_{om,CEC} w_{om}\right)\right] \qquad (15).$$

Materials and methods

Study area

The semi-empirical model was applied to the irrigated agricultural area of the Vega Baja del Segura and Baix Vinalopó (SE Spain) which amounts to 55,000 ha of land (Fig. 1). The soils in this area are mostly calcaric Fluvisols in the alluvial central part and, additionally, various types of Calcisols, Regosols and gleyic Solonchaks to the outskirts (Ortiz et al., 2008). Surface textures range from silt loam to silty clay loam and clay mineralogy overwhelmingly correspond to hydrated micas. According to the Thornthwaite and Köppen-Geiger systems, the climate in the area is classified as arid to semi-arid hot-summer Mediterranean, i.e., very dry with hot summers and mild winters and where the scarce rainfalls concentrate mainly in autumn and then spring and winter (Fig. 2).

[Figure 1]

[Figure 2]

Soil surveys

Two surveys were carried out four years apart. The first one was made in summer 2006 when 28 sites distributed in the whole study area were visited. The second one was made in autumn 2010 when another set of 28 sites were visited following 75 mm of rainfall in the area since mid August (Fig. 2). Ten of these had been already visited in summer 2006, specifically they were within a radius of 250 m of one previous site, whereas the other 18 were further away (Fig. 1). The 28 selected sites in 2006 and the new 18 sites in 2010 were distributed, respectively, in the whole study area (2006) and only in the central alluvial part (2010) according to two systematic random sampling designs using a Geographic Information System (GIS). The sites from the first survey were used for calibration and cross-validation of the model, whereas the sites from the second survey were used for external validation.

Soil water content and salinity are very dynamic and hence time-variable in irrigated agricultural fields, overall under dry sub-humid to arid climates. Therefore, by changing the seasons between the first and second surveys we aimed at maximizing differences of water content and salinity between calibration and validation.

EMI instrument

The EMI instrument used in this work was the EM38 (Geonics Ltd., Mississauga, Ontario, Canada). The EM38 primary magnetic field frequency (f = 14.6 kHz) and spacing between the transmitter and receiver coils (r = 1 m) enables it to respond to the conductive properties of ground materials, and barely to their magnetic properties, down to 0.8 and 1.5 m for 75% cumulative signal in, respectively, the horizontal (H) and vertical (V) coplanar 'dipole' orientations (McNeill, 1980). These characteristics make it especially suitable for the sensing of σ_b in the rooting depth of most crop plants.

EMI measurements

A global positioning system (GPS) receiver was used to locate the exact selected site. Before taking the EMI measurements in each site, the EM38 instrument functioning parameters were adjusted in order to avoid the drift effects known to affect this device (Sudduth et al., 2001). According to the EM38 instructions manual (Geonics Ltd., 1992), first of all, the instrument was left to warm-up away from direct sunlight for 15 minutes on a homogeneous expanse of low-conductive ground outside the target agricultural site, i.e., a shaded spot on the access road. Then, the in-phase and quadrature-phase measurements were set to zero by adequately switching the I/P and

Q/P controls. Finally, the EM38 was lifted to 1.5 m height and the Q/P control was switched again to have a σ_b* measurement in the vertical dipole mode double than in the horizontal one at that height.

After setting up the instrument, the σ_b* of the soil in the selected site was measured with the EM38 in both available dipole orientations, i.e., V and H, and at 0, 50, 100, 150 and 200 cm over the ground to compile a set of ten measurements per site: $\sigma_{b(V0)}$*, $\sigma_{b(V50)}$*, $\sigma_{b(V100)}$*, $\sigma_{b(V150)}$*, $\sigma_{b(V200)}$*, $\sigma_{b(H0)}$*, $\sigma_{b(H50)}$*, $\sigma_{b(H100)}$*, $\sigma_{b(H150)}$* and $\sigma_{b(H200)}$*.

Soil sampling, bulk electrical conductivity and temperature measurements

After the EMI measurements, the soil beneath the centre of the instrument in each site was drilled with a Riverside auger 10 cm in diameter. Four disturbed samples were separately taken from the upper topsoil, lower topsoil, subsurface soil and subsoil and sealed in plastic bags. In the first survey the depth intervals were, respectively, 0-10, 10-30, 30-65 and 65-95 cm, and in the second one were 0-10, 10-30, 30-60 and 60-90 cm.

Besides, in the second survey, a second point next to the first one was drilled to take undisturbed soil cores 5 cm in diameter and height with a 0753SA volumetric sampler (Eijkelkamp, Giesbeek, The Netherlands) from the depth intervals 0-5, 10-15, 30-35 and 50-55 cm. The values for the ranges 0-10, 10-30 and 30-60 cm were hence calculated by means of linear interpolation from the values determined at 0-5, 10-15, 30-35 and 50-55 cm. Additionally, an average bulk density for the depth interval 60-90 cm could be calculated by non-linear extrapolation using the following potential function calibrated with the shallower depth intervals:

$$\rho_b = 1.1428\ z^{0.08} \qquad (16),$$

which gave 1.61 g cm^{-3} and was subsequently used as the ρ_b of the 60-90 cm layer in all the sites of the second survey for the external validation. Besides, the mean ρ_b values obtained for the 0-10, 10-30 and 30-60 cm soil layers in the second survey, in addition to the previously commented ρ_b value for the 60-90 cm soil layer, were used for, respectively, the 0-10, 10-30, 30-65 and 65-95 cm soil layers in the calibration and cross validation of the model for σ_b* prediction.

In both soil surveys, as the soil was drilled to take the disturbed soil samples, the bulk electrical conductivity and temperature were measured at the following depths: 0, 10, 30 and 50 cm with a WET-2 sensor (Delta-T Devices Ltd., Cambridge, UK). Temperature was empirically modelled in each site as a function of depth (z) with this equation:

$$t = \alpha\, z^{\beta} \qquad (17),$$

and as a consequence, a t estimate could be made for the subsoil layers.

Soil analyses

The soil samples from the first survey were, first of all, analysed for the mass fraction of water at field conditions (w_w) by oven-drying during 24 h at 105 ºC of a representative subsample 20 g in weight.

The undisturbed soil cores from the validation sampling were oven-dried at 105 ºC for 24 h, weighted and then, the w_w and bulk density (ρ_b) determined. These were the only determinations made in these undisturbed cores.

Following the w_w determination, all disturbed soil samples were spread out on trays and left to dry at room air conditions. Then, they were gently deaggregated to pass a 2-mm mesh sieve and the air-dry fine earth saved for the analyses explained in the ensuing paragraphs.

The soil organic matter mass fraction (w_{om}) was determined according to the Walkley and Black method using a Walkley-Black factor of 1.282, which is based on the assumption that only 78% of soil OM reacts in the mild oxidation conditions featuring this method, and a van Bemmelen factor of 1.724, which is based on the hypothesis that soil OM is 58% carbon (Nelson & Sommers, 1996).

The soil texture, and thus clay mass fraction (w_c) was determined with the hydrometer method (Gee & Or, 2002) using $NaPO_3$ 0.25% (w/v) in water as dispersing medium and 20 g of air-dry fine earth.

The saturated paste was prepared by adding deionized water (~ 1 µS cm^{-1}) to 400 g of air-dry fine earth (Rhoades, 1996). Then, the soil water was vacuum extracted and the σ_e immediately measured with a microCM 2201 conductimeter (Crison, Barcelona, Spain) equipped with a 1.1 cm^{-1} cell and a temperature probe.

Model application

To calibrate and validate the model presented in this work, first of all, a 1D inversion was performed on Eq. 2 to obtain the σ_b values at different soil depths from the σ_b* at different heights collected in the first survey. Then, Eq. 15 was calibrated employing the basic ground properties in the first survey and hence the optimum values of the parameters a, b and B obtained (Fig. 3 top row). Once calibrated, Eq. 15 was used to estimate the σ_b at different depths from the basic ground properties in the second survey. Finally, Eq. 2 was forwardly applied to calculate the σ_b* at different heights in the second survey from the estimates of σ_b, and the σ_b* calculations were compared to the EM38 measurements for validation (Fig. 3 bottom row).

[Figure 3]

Calculation of the σ_b of the different soil layers from the σ_b measurements at different heights*

According to the model presented by means of Eq. 2, the EMI-surveyed soils can be conceptually split in n layers ($n \leq 2\,m$), each one characterized by a σ_b value, and this set of n σ_b values, in our case $n = 5$ and, therefore [$\sigma_{b0\text{-}10}$, $\sigma_{b10\text{-}30}$, $\sigma_{b30\text{-}60(65)}$, $\sigma_{b60(65)\text{-}90(95)}$, $\sigma_{b>90(95)}$], can be calculated by inversion of the matrix of sensitivity coefficients, followed by multiplication by the vector of σ_b* measurements, in our case [$\sigma_{b(V0)}$*, $\sigma_{b(V50)}$*, $\sigma_{b(V100)}$*, $\sigma_{b(V150)}$*, $\sigma_{b(V200)}$*, $\sigma_{b(H0)}$*, $\sigma_{b(H50)}$*, $\sigma_{b(H100)}$*, $\sigma_{b(H150)}$*, $\sigma_{b(H200)}$*]. Although correct, this problem is, however, ill-posed. That is, because all the σ_b* measurements are often highly correlated, the solution is remarkably sensitive to small deviations in the σ_b* measurements, thus leading to non-reproducible results. This difficulty can be conveniently overcome using the Tikhonov regularization (Zhdanov, 2018). In this approach the minimum of the following objective function Φ_A (Eq. 18) is iteratively searched using different values of the λ parameter at a time (Borchers et al. 1997; Hendrickx et al., 2002):

$$\Phi_A = \sum_{i=1}^{2m} (\sigma_{b(Xh_i)}{*} - \sigma_{b(Xh_i)}{*'})^2 + \lambda^2 \sum_{j=1}^{n}\sum_{k=1}^{n} (l_{jk}\sigma_{b(d_k)})^2 \quad (18)$$

where X is V or H, $\sigma_{b(Xhi)}$*’ is the predicted $\sigma_{b(Xhi)}$* and l_{jk} is the element of the jth row and kth column of the second derivative matrix **L** (Eq. 19):

$$\mathbf{L} = \begin{bmatrix} -2 & 1 & 0 & \dots & 0 \\ 1 & -2 & 1 & \dots & 0 \\ 0 & 1 & -2 & \dots & 0 \\ \dots & \dots & \dots & \dots & 1 \\ 0 & 0 & 0 & 1 & -2 \end{bmatrix} \quad (19).$$

In order to search for an adequate λ value, the range from 0.07 to 3 is usually tested (Huang et al., 2017; Dakak et al., 2017). In this work the 0-to-2 interval was explored instead, where a $\lambda = 0$ transforms the objective function Φ_A in a least-squares one. The adequate λ value in this work was selected by taking the one that featured the vertex of the 'L' shaped graph that arises by representing the first against the second summand of the objective function Φ_A (Borchers et al., 1997; Hendrickx et al., 2002). Note that the Tikhonov regularization was independently applied for each location in the surveys and, therefore, a different λ value for each one was obtained and subsequently used to calculate its corresponding set of n σ_b values.

Following the calculation of the n σ_b values for each site, they were compared with the σ_b values measured with the WET-2 so as to know the degree of applicability of the linear model represented by Eq. 2 in the soils of the study area. The soil weighted σ_b averages were also assessed with Eq. 6, and the induction numbers N_B next calculated with Eq. 5.

Calibration of the model for σ_b prediction*

Once the σ_b of the different soil layers in every site belonging to the first survey had been calculated, Eq. 15 was calibrated using the values of σ_e, θ_w, w_c, w_{om} and t that had been determined for the same soil layers. For ρ_b the mean value for every soil layer obtained in the second soil survey was used. Therefore, the calibration of Eq. 15 consisted in finding the values of the parameters a, b and B that minimized the sum of square errors between measured ($\sigma_{b(dko)}$) and calculated ($\sigma_{b(dko)}$') soil bulk electrical conductivities for all sites and soil layers (Φ_B):

$$\Phi_B = \sum_{o=1}^{28} \sum_{k=1}^{n} (\sigma_{b(d_{ko})} - \sigma_{b(d_{ko})}')^2 \qquad (20).$$

The other seven parameters in Eq. 15 (σ_{p0}, k_σ, w_{e0}, $k_{c,e}$, CEC_0, $k_{c,CEC}$ and $k_{om,CEC}$) were not estimated by means of the Φ_B minimization since they were known from other works of the study area where they have been calculated by simple linear regression of the equations they specifically feature, i.e., Eq. 11, Eq. 12 and Eq. 14 (Table 2).

[Table 2]

Estimation of confidence intervals for the a, b and B coefficients

The 95% confidence intervals for the coefficients a, b and B were determined by means of the bootstrapping percentile method in which 1000 bootstrap replications of size 28 × 4 = 112 were drawn from the calibration dataset. Then, the a, b and B coefficients of each one were calculated and the 2.5th and 97.5th percentiles finally assessed (Devore & Berk, 2018).

Cross-validation of the model for σ_b* *prediction*

A leave-one-site-out scheme was used for cross-validation of the model with the data from the first survey. In the first survey dataset, one location was removed at a time and the parameters a, b and B each time recalculated with the other 27 sites. Then, the σ_b in the layers 0-10, 10-30, 30-65, 65-95 and below 95 cm ($\sigma_{b(0\text{-}10)}$, $\sigma_{b(10\text{-}30)}$, $\sigma_{b(30\text{-}65)}$, $\sigma_{b(65\text{-}95)}$ and $\sigma_{b(>95)}$) of the removed site were predicted using the recalculated a, b and B values. Finally, these newly predicted σ_b values were used along with Eq. 2 to calculate the σ_b* that would have resulted from the measurement with the EM38 in the vertical and horizontal dipole orientations and at 0, 50, 100, 150 and 200 cm height, and were compared to the observed values.

External validation of the model for σ_b* *prediction*

The model parameters a, b and B that had been estimated in the calibration of Eq. 15 were used along with this equation and the soil properties (σ_e, θ_w, w_c, w_{om}, ρ_b and t) that had been determined in the different layers of the 28 sites of the second survey to predict σ_b at 0-10, 10-30, 30-60, 60-90 and below 90 cm ($\sigma_{b(0\text{-}10)}$, $\sigma_{b(10\text{-}30)}$, $\sigma_{b(30\text{-}60)}$,

$\sigma_{b(60\text{-}90)}$ and $\sigma_{b(>90)}$) (Fig. 3 from top to bottom row). Then, calculated and WET-2-measured σ_b values were compared, and Eq. 2 was used to calculate the σ_b* that would have been obtained in the vertical and horizontal dipole orientations and at 0, 50, 100, 150 and 200 cm height.

Results

EMI measurements

The EMI measurements (Visconti & de Paz, 2020) always decreased as height increased both in the vertical and horizontal dipole modes and in both surveys (Fig. 4). They ranged from 0.01 to 2.47 dS/m in the first survey and from 0.01 to 3.44 dS/m in the second one, i.e., the σ_b* measurements in the first survey were consistently lower than in the second one (SIM 2). Conversely, the quotient $\sigma_{b(H0)}$*/$\sigma_{b(V0)}$* was higher (0.98) in the first than in the second survey (0.77), which indicates that the σ_b profile was more homogeneous in the first survey than in the second one.

[Figure 4]

The Pearson's skewness coefficients for all measurements and both surveys were well within the [-1, 1] limits and thus, normality could be assumed for all σ_b* measurements.

From Fig. 4 it is apparent that, in general, the higher the measurement at the soil surface, the higher the measurement at whatever height. This visual observation was supported by the correlation coefficients: the Pearson's product-moment correlation coefficients among the σ_b* measurements at the different soil heights and dipole modes were between 0.881 and 0.994 in the first survey and between 0.894 and 0.995 in the second one (SIM 3).

Soil properties

The σ_e values measured in the first survey were higher than in the second one, and the difference between both was, in general, larger near surface (SIM 4). Interpretation of these observations points towards the effect of the season each survey was carried out. The first one was performed in summer when soil salinity is expected to be higher because of the high evapotranspiration, rainfall scarcity characteristic of the Mediterranean climate in the area during summer and, hence, plenty of irrigations and salt inputs to the soils therein. On the contrary, the second survey was made in autumn when soil salinity is expected to be lower because of the much lower evapotranspiration in that season and the leaching effect of the autumn rainfalls featuring again the Mediterranean climate in the area and which, in 2010 amounted to 75 mm (Fig. 2).

Additionally, the effect of the different season each survey was carried out showed up in θ_w (SIM 4). As expected, soil water contents were lower in the first survey, which was carried out in summer, than in the second autumnal one and, again, the shallower the soil the wider the difference.

Regarding the clay and OM mass fractions, i.e., w_c and w_{om}, these were, in general, higher in the first survey (SIM 4). This is likely due to the fact that the sites of the second survey were more clustered in the alluvial part of the study area where the soils have finer textures and, as a consequence of this characteristic, they are also a bit higher in organic matter (Fig. 1).

Regarding the bulk density, this was only determined in the second survey and not for exactly the same depth intervals that σ_e, θ_w, w_c and w_{om}. It increased from the upper topsoil to the subsurface soil layer with barely variations from there down (SIM 4).

Finally, regarding the WET-2 measurements, both σ_b and temperature were higher in the first survey, which was carried out in summer, than in the second one, that so was in autumn (SIM 5). Differences between the summer and autumn soil temperatures were between 18 and 11 ºC: the highest within the shallowest soil depth.

Regarding distributions, σ_e and w_{om} were the properties which presented more skewness coefficients outside the [-1, 1] bounds. Additionally, the logarithmic transformations (to base 10) of both variables were able to give distributions, in general, less skewed (SIM 4), thus indicating that these properties tend to be log-normally distributed in the area.

Calculation of the σ_b of the different soil layers from the σ_b measurements at the different heights*

Since the σ_b* measurements at the different heights were highly correlated (SIM 3), a traditionally least-squares minimization to solve Eq. 2 could not be applied. Alternatively, the Tikhonov regularization was done.

In the Tikhonov regularization the λ parameters featuring the vertex of the graph of the first against the second summand of Eq. 18 were between 0.34 and 0.75 in the first survey with mean of 0.44 ± 0.03 (Table 3). Once the adequate λ values for each site had been calculated, Eq. 2 could be inverted and the σ_b at the different soil depths at each site in the first survey calculated from the corresponding sets of σ_b* measurements at the different heights.

[Table 3]

For the soils that were highly conductive, their σ_b increased from the upper topsoil down to the subsurface soil and then, it kept almost constant with depth, i.e., σ_b followed a ‘normal’ conductivity profile (Fig. 5). Conversely, for soils that were lowly conductive, their σ_b kept almost constant from the topsoil down to the subsoil, i.e., σ_b followed a 'uniform' conductivity profile (Fig. 5). Inverted conductivity profiles were not observed. In any case, the σ_b values at the different soil depths were highly correlated featuring Pearson's product-moment correlation coefficients between 0.950 and 0.997 in the first survey. This high correlations logically follow those also observed in the σ_b* measurements at the different heights and dipoles over the ground (SIM 3).

[Figure 5]

Next, depth-weighted σ_b averages ($\overline{\sigma_b}$) were obtained for each of the sites with Eq. 6 (Table 3), and the induction number (N_B) was thus calculated with the use of Eq. 5 where r, μ_0 and ω are all known. The N_B values were between 0.029 and 0.101 with mean of 0.059 ± 0.008 in the first survey and somewhat higher in the second one (Table 3). These induction numbers are at least one order of magnitude below unity, however, in order to know whether they are low enough to adequately fulfil the requirement of low induction numbers ($N_B << 1$), the σ_b values calculated by means of the 1D inversion were compared to the WET-2 σ_b measurements giving R^2 of 0.59 and RMSE of 0.17 dS/m (19%). However, what was more relevant is that the calculations were on average very similar to the measurements (Fig. 6a) with a mean pairwise difference of -0.07 ± 0.10 dS m^{-1}, which is not different from zero at the 95% confidence level (p = 0.13). This fact gave support to the hypothesis of low induction numbers and the convenience of the linear model represented by Eq. 2 for the soils of the study area.

[Figure 6]

Calibration of the model

The calibration of the model given by Eq. 15 was done using the σ_b values previously calculated by the 1D inversion of Eq. 2 for all the sites in the first survey (Fig. 5). As a consequence, the following estimations for the 95% confidence intervals of the a, b and B parameters in Eq. 15: a = 0.51 ± 0.23, b = 0.09 ± 0.07, and B = (1.3 ± 0.7) × 10^{-6} S m^2 $mmol_C^{-1}$ were obtained.

The calibrated values of a, b and B, along with the rest of coefficients in Eq. 15 (Table 2), were used to predict σ_b at the different soil depths in each site of the first survey. On the basis of these σ_b values, the corresponding σ_b* at the different heights over the ground in each site of the first survey were subsequently calculated with the forward application of Eq. 2.

The fit of predictions against measurements for σ_b* in the horizontal and vertical dipole modes is shown in Fig. 7a and b. The coefficient of determination (R^2) and RMSE of the model for σ_b* prediction in the vertical dipole mode for all measurements were 0.84 and 0.18 dS m^{-1} (41%), respectively, whereas the R^2 and RMSE in the horizontal one were 0.90 and 0.11 dS m^{-1} (39%), also respectively (Table 4). The mean pairwise difference between predictions and observations was -0.04 ± 0.03 dS m^{-1} in the vertical dipole, i.e., different from zero at the 95% confidence level ($p = 0.006$), and 0.007 ± 0.018 dS m^{-1} in the horizontal dipole, i.e., non-different from zero at the 95% confidence level ($p = 0.4$). The fit between measurements and predictions barely changed as a function of the measurement height as revealed by the R^2 and RMSE percentages (Table 4).

[Figure 7]

[Table 4]

Cross-validation of the model

The fit of predictions against observations of σ_b* in the horizontal and vertical dipole modes at 0, 50, 100, 150 and 200 cm height is shown in Fig. 7c and d. The coefficient of determination (R^2) and RMSE of the model for σ_b* prediction in the vertical dipole mode were for all measurements, respectively, 0.80 and 0.19 dS m^{-1} (43%), whereas the R^2 and RMSE in the horizontal one were, respectively, 0.87 and 0.12 dS m^{-1} (43%), respectively (Table 4). The mean pairwise difference between predictions and observations was -0.04 ± 0.03 dS m^{-1} in the vertical dipole, i.e., different from zero at the 95% confidence level ($p = 0.02$), and 0.01 ± 0.02 dS m^{-1} in the horizontal dipole, i.e., non-different from zero at the 95% confidence level ($p = 0.3$).

External validation of the model

The model in Eq. 15 with calibrated parameters a, b and B was applied to the basic ground data from the second survey to predict the σ_b at the different soil depths. The fit of predictions against WET-2 measurements presented R^2 of 0.65 and RMSE of 0.13 dS m^{-1} (15%) (Fig. 6b) therefore slightly improving precision regarding what had been obtained in the 1D inversion (Fig. 6a). However, accuracy decreased with a mean pairwise difference between predictions and observations of 0.17 ± 0.08 dS m^{-1}, i.e., significantly different from zero at the 95% confidence interval ($p < 0.001$).

Then, by the forward application of Eq. 2 the σ_b* data were calculated. The fit of predictions against observations of σ_b* in the horizontal and vertical dipole modes at 0, 50, 100, 150 and 200 cm height is shown in Fig. 7e and f. The coefficient of determination (R^2) and RMSE of the model for σ_b* prediction in the vertical dipole mode were for all measurements 0.80 and 0.24 dS m^{-1} (44%), respectively, whereas the R^2 and RMSE in the horizontal one were 0.90 and 0.13 dS m^{-1} (38%), respectively (Table 4). The mean pairwise difference between predictions and observations was -0.12 ± 0.06 dS m^{-1} in the vertical dipole, i.e., different from zero at the 95% confidence level ($p < 0.001$), and 0.008 ± 0.200 dS m^{-1} in the horizontal dipole, i.e., non-different from zero at the 95% confidence level ($p = 0.5$). Again, the fit between measurements and predictions barely changed as a function of measurement height as revealed by the R^2 and RMSE percentages (Table 4).

Discussion

There are many models for the prediction of one of the following five basic soil properties: σ_e, θ_w, w_c, w_{om} and ρ_b on the basis of EMI measurements. All these models are purely empirical and usually calibrated by means of simple linear regression (e.g., McKenzie et al., 1989), multiple linear regression (e.g., Díaz and Herrero, 1992), or either geostatistical techniques (e.g., García-Tomillo et al., 2017). There are also consolidated mathematical techniques for the calculation of soil σ_b values from EMI measurements (Zhdanov, 2018) which have been compared to TDR-measured σ_b values (Dragonetti et al., 2018). In this work, however, a semi-empirical model was developed to predict, not the basic properties, but the EMI measurements themselves, specifically, the EM38 measurements at the two dipole orientations and various heights over the ground on the basis of the main five soil properties, besides temperature, on which soil conductivity depends at various depths.

This semi-empirical model presents two parts: one that relates the σ_b* measurements at the different dipoles and heights with the σ_b values at the different soil depths (Eq. 2) and another that relates the σ_b values to the soil properties (Eq. 15). The linearity of Eq. 2 has eased the model development, however, it is an approximation that only holds for low induction numbers, i.e., when the ability of the soil to attenuate the primary magnetic field of the EMI instrument conforms to the asymptotic approximation of Maxwell's equations developed by McNeill (1980). If this approximation is valid then the σ_b values calculated by inversion of Eq. 2 are considered to adequately correspond to true σ_b values (Callegary et al., 2007), i.e., those that would be measured by a reliable direct contact technique, mainly ER, but also TDR and FDR. In this work the σ_b values obtained by inversion of Eq. 2 have been compared with the σ_b measurements taken with the WET-2, an FDR sensor, and, though featuring a remarkable scattering, have been found to satisfactorily agree on average. Even though relevant, the scattering is a consequence of the different sensing volumes of the WET-2 and the EM38, which are, respectively, 0.5 dm^3 and 1000 dm^3 according to their instructions manuals and, therefore, as already pointed out by Coppola et al. (2016) when calibrating EMI with TDR measurements, while the WET-2 provides quasi-point-like measurements and thus does not integrate the small-scale soil variability, the EM38 integrates all the small-scale soil heterogeneities. In short, the lack of bias in the σ_b estimation gave us confidence that the low induction number hypothesis is acceptably fulfilled in the surveyed soils featuring estimated N_B values between 0.029 and 0.101 with mean of 0.059.

In the calibration of the semi-empirical model developed in this work, the R^2 coefficients for σ_b* prediction were between 0.84 and 0.90, with the lower value corresponding to the vertical dipole measurements and the higher to the horizontal one. The magnitude of the R^2 values found in this work are similar to the 0.92 for the vertical and the 0.83 for the horizontal dipole modes found by Brevik and Fenton (2002), who developed a multiple linear regression model for the EM38 measurements using θ_w, w_c, t and the carbonate mass fraction as predictors.

The predictive ability of the semi-empirical model developed in this work decreased a bit when it was externally validated for the vertical dipole mode but not at all for the horizontal one. However, since σ_e and θ_w were on average 23% lower and 23% higher, respectively, in the second validation survey regarding the first calibration one, the result of this validation means that the model seems to not depend much on the average values of these properties, although this should be rigorously assessed with a sensitivity analysis. In addition to σ_e and θ_w, the soil temperature also changed from calibration to validation: it was, on average, between 18 and 11 ºC higher in the first calibration survey in comparison to the second validation one. Therefore, the model resisted this change too without losing much accuracy. Besides, the better performance in the horizontal dipole mode corresponds well with the higher sensitivity of the EM38 to the shallower soil layers in this measurement orientation. Considering additionally, the soil conductivity profile was more homogeneous in the first survey than in the second one, the validation conditions, on the whole, were very challenging thus giving us more confidence in the ability of the model to grab the underlying EMI signal generating process. Even more, since in inverted soil conductivity profiles, the shallower the soil layer the more conductive, the model developed in this work would be expected to behave even better with inverted conductivity profiles. This way we can say that the model is able to represent the soil as a conductive system under EMI.

Out of the ten parameters of the semi-empirical model developed in this work, only the three related to tortuosity (a and b) and the exchange complex (B) were estimated in the calibration. The parameters a and b presented values of 0.51 ± 0.23 and 0.09 ± 0.07. These are, respectively, slightly lower and higher in comparison to those in Rhoades et al. (1976) and Kelleners and Verma (2010) that were between 1.4 and 2.1 and between -0.27 and -0.09. Nevertheless, they are within the intervals estimated by Visconti et al. (2014) for the upper topsoil layer of a site within the same study area using instead of EMI, FDR and capacitance-conductance techniques, which were, respectively, between 0 and 6 and between 0.8 and -1. Regarding, the equivalent conductance of the counterions on the exchange complex, the value obtained in this work was $(1.3 \pm 0.7) \times 10^{-6}$ S m^2 mmol$_C^{-1}$, i.e., one order of magnitude lower than the value obtained by Kelleners and Verma (2010) for a loamy soil, which was 5.9×10^{-5} S m^2 $mmol_C^{-1}$. This remarkable departure could be caused by the sites where the hypothesis of low induction numbers is less acceptable.

The development of a semi-empirical model of the form $\sigma_b^* = \sigma_b^*(\sigma_e, \theta_w, w_c, w_{OM}, \rho_b)$ in which σ_b^* is taken as an effect that depends on several causes, i.e., basic soil properties, has given insight into how these contribute to the building of the EMI signal. That is, that the dependence of the EMI signal on the several basic soil properties is essentially linear with, perhaps, the exception of θ_w, whose dependence may be regarded as quadratic since it appears in both factors of Eq. 15. Contrary to this semi-empirical model, a classical one of the type $x = f(\sigma_b^*, y_1, y_2, ...)$ where the dependent variable x is either σ_e, θ_w, w_c, w_{OM} or ρ_b, and the y's are whichever of the basic properties that are not the target one and/or other measurements, takes linearity for granted and aims at just estimation of the target property.

The practical interest of the semi-empirical model developed in this work is that the σ_b profile of the soils and, therefore, the induction numbers and the σ_b^* measurements can be estimated in advance thus providing information about the applicability and scope of the technique in a study area as a part of the survey planning. Moreover, the sensitivity analysis of this model for an area will provide beforehand information about which properties will influence the most the sensor signal thus contributing to know if it is worth to perform a survey for one soil property if other soil properties are more influential than that.

Conclusions

A semi-empirical model to predict the measurements taken with an EMI device, specifically the EM38 in the horizontal and vertical dipole modes, and at various heights from 0 up to 200 cm over the ground, was developed using the soil contents of salt, water, clay and organic matter, in addition to bulk density and temperature, at various soil depths, as predictors. Since the hypothesis of low induction numbers was acceptably fulfilled in the study area, the model could be calibrated and validated with the data obtained therein, respectively, in two contrasted seasons. This model presented coefficients of determination between 0.8 and 0.9 in the calibration, cross-validation and external validation analyses, RMSE values between 38 and 44% and, mean pairwise differences between -0.04 ± 0.03 and -0.12 ± 0.06 dS m^{-1} for the vertical dipole and between 0.007 ± 0.018 and 0.01 ± 0.02 dS m^{-1} for the horizontal one. The model significantly underestimated ($p < 0.05$) the EM38 measurements in the vertical dipole, but not in the horizontal one. Remarkably, however, the model was robust against changes in the mean soil contents of salt, water, and temperature and, also against changes in the conductivity profile shape, from the calibration to the external validation. Even though the robustness of the model against changes in the mean and variability of the basic soil properties can only be rigorously tested by means of a sensitivity analysis, the stability from calibration to validation gave us confidence on the model predictive ability for conditions differing from the calibration. As a consequence, this model helps to understand how the different soil properties physically contribute to conductivity and why calibrations are so site-specific in the practice of EMI soil surveying. For the study area for which it was developed, the model can be used to advance the EMI measurements taken with the EM38 at different heights and dipole orientations. Notwithstanding this, by replacement of the values of its parameters for the ones that characterize other study areas it may also be used elsewhere for the estimation of σ_b profiles, induction numbers and σ_b* measurements and, additionally, to estimate the importance the different basic soil properties have on the EM38 signal. In future works, the model here presented will be subjected to a sensitivity analysis in order to ascertain the relative importance of the soil properties on the EMI measurements. It will be also extended to other instruments and areas, thus testing its universality.

Acknowledgements

The first survey of this project was carried out within project GV 0461/2006, funded by the *Generalitat Valenciana*, and the second one within projects CGL2009-14592-C02-01 and CGL2009-14592-C02-02 funded by the *Ministerio de Ciencia e Innovación* from the Government of Spain and additionally within project Val i+d APOSTD/2010/029 (F. Visconti), funded by the *Generalitat Valenciana*.

Conflicts of interest

The authors declare that they have no conflicts of interest.

Data availability

The data associated to this article is stored in the public repository Mendeley Data (https://data.mendeley.com/): Visconti, Fernando; de Paz, José Miguel (2020), "Soil and electromagnetic induction surveys in the Vega Baja del Segura and Baix Vinalopó in 2006 and 2010", Mendeley Data, V1, doi: 10.17632/rh729nhdz3.1. They will be made openly accessible from 20th October 2020 on.

References

Bell, M.A., & van Keulen, H. (1995). Soil pedotransfer functions for four Mexican soils. *Soil Science Society of America Journal*, 59, 865–871.

Borchers, B., Uram, T., & Hendrickx, J.M.H. (1997). Tikhonov regularization of electrical conductivity depth profiles in field soils. *Soil Science Society of America Journal*, 61, 1004–1009.

Brevik, E.C., & Fenton, T.E. (2002). Influence of soil water content, clay, temperature, and carbonate minerals on electrical conductivity readings taken with an EM-38. *Soil Survey Horizons Spring*, 9–13.

Brevik, E.C., Fenton, T.E., & Lazari, A. (2006). Soil electrical conductivity as a function of soil water content and implications for soil mapping. *Precision Agriculture*, 7, 393–404.

Callegary, J.B., Ferré, T.P.A., & Groom, R.W. (2007). Vertical spatial sensitivity and exploration depth of low-induction-number electromagnetic-induction instruments. *Vadose Zone Journal*, 6(1), 158–167.

Carter, L.M., Rhoades, J.D., & Cesson, J.H. (1993). Mechanization of soil salinity assessment for mapping. Winter Meetings of the American Society of Agricultural Engineers, Paper No. 931557, St. Joseph (Michigan): American Society of Agricultural Engineers.

Coppola, A., Smettem, K., Ajeel, A., Saeed, A., Dragonetti, G., Comegna, A., Lamaddalena, N., & Vacca, A. (2016). Calibration of an electromagnetic induction sensor with time-domain reflectometry data to monitor rootzone electrical conductivity under saline water irrigation. *European Journal of Soil Science*, 67 (6), 737 – 748.

Corwin, D.L., & Lesch, S.M. (2005). Apparent soil electrical conductivity measurements in agriculture. *Computers and Electronics in Agriculture*, 46, 11–43.

Corwin, D.L., & Rhoades, J.D. (1990). Establishing soil electrical conductivity-depth relations from electromagnetic induction measurements. *Communications in Soil Science and Plant Analysis*, 21(11-12), 861– 901.

Cox, D.R. (2006). Principles of Statistical Inference. Cambridge: Cambridge University Press.

de Jong, E., Ballantyne, A.K., Cameron, D.R., & Read, D.W.L. (1979). Measurement of apparent electrical conductivity of soils by an electromagnetic induction probe to aid salinity surveys. *Soil Science Society of America Journal*, 43(4), 810–812.

Dakak, H., Huang, J., Zouahri, A., Douaik, A., & Triantafilis, J. (2017). Mapping soil salinity in 3-dimensions using an EM38 and EM4Soil inversion modelling at the reconnaissance scale in central Morocco. *Soil Use and Management*, 33(4), 553–567.

Devore, J.L., & Berk, K.L. (2018). Modern Mathematical Statistics with Applications 2nd Ed. New York: Springer.

Díaz, L., & Herrero, J. (1992). Salinity estimates in irrigated soils using electromagnetic induction. *Soil Science*, 154(2), 151–157.

Doolittle, J., Petersen, M., & Wheeler, T. (2001). Comparison of two electromagnetic induction tools in salinity appraisals. *Journal of Soil and Water Conservation*, 56(3), 257–262.

Dragonetti, G., Comegna, A., Ajeel, A., Piero Deidda, G., Lamaddalena, N., Rodriguez, G., Vignoli, G., & Coppola, A. (2018). Calibrating electromagnetic induction conductivities with time-domain reflectometry measurements. *Hydrology and Earth System Sciences*, 22(2), 1509–1523.

Freeland, R.S., Yoder, R.E., Ammons, J.T., & Leonard, L.L. (2002). Mobilized surveying of soil conductivity using electromagnetic induction. *Applied Engineering in Agriculture*, 18(1), 121–126.

García-Tomillo, A., Mirás-Avalos, J.M., Dafonte-Dafonte, J., & Paz-González, A. (2017). Estimating soil organic matter using interpolation methods with a electromagnetic induction sensor and topographic parameters: a case study in a humid region. *Precision Agriculture*, 18(5), 882–897.

Gee, G.W., & Or, D. (2002). Particle-size analysis. In: G. Campbell, R. Horton, W.A. Jury, D.R. Nielsen, H.M. van Es, P.J. Wierenga, J.H. Dane & G.C. Topp. (Eds.), Methods of Soil Analysis. Part 4. Physical Methods (pp. 255–294). Madison (Wisconsin): SSSA, ASA.

Geonics Ltd. (1992). Geonics EM38 Ground Conductivity Meter Operating Manual. Ontario (Canada): Geonics Limited.

Hedley, C.B., Yule, I.J., Eastwood, C.R., Shepherd, T.G., & Arnold, G. (2004). Rapid identification of soil textural and management zones using electromagnetic induction sensing of soils. *Australian Journal of Soil Research*, 42(4), 389–400.

Heil, K., & Schmidhalter, U. (2017). The application of EM38: Determination of soil parameters, selection of soil sampling points and use in agriculture and archaeology. *Sensors*, 17(11), 2540 (1–44).

Hendrickx, J.M.H., Borchers, B., Corwin, D.L., Lesch, S.M., Hilgendorf, C., & Schlue, J. (2002). Inversion of soil conductivity profiles from electromagnetic induction measurements theory and experimental verification. *Soil Science Society of America Journal*, 66, 673–685.

Huang, J., Ramamoorthy, P., McBratney, A., & Bramley, H. (2018). Soil water extraction monitored per plot across a field experiment using repeated electromagnetic induction surveys. *Soil Systems*, 2(11), 1–17.

Huang, J., Kilminster, T., Barrett-Lennard, E.G., & Triantafilis, J. (2017). Characterization of field-scale dryland salinity with depth by quasi-3d inversion of DUALEM-1 data. *Soil Use and Management*, 33(2), 205–215.

Jung, W.K., Kitchen, N.R., Sudduth, K.A., Kremer, R.J., & Motavalli, P.P. (2005). Relationship of apparent soil electrical conductivity to claypan soil properties. *Soil Science Society of America Journal*, 69, 883–892.

Jurinak, J.J., Sandhu, S.S., & Dudley, L.M. (1987). Ionic diffusion coefficients as predicted by conductometric techniques. *Soil Science Society of America Journal*, 51, 625–630.

Kachanoski, R.G., Gregorich, E.G., & Van Wesenbeeck, I.J. (1988). Estimating spatial variations of soil water content using noncontacting electromagnetic inductive methods. *Canadian Journal of Soil Science*, 68(4), 715–722.

Kelleners, T.J., Soppe, R.W.O., Ayars, J.E., & Skaggs, T.H. (2004). Calibration of capacitance probe sensors in a saline silty clay soil. *Soil Science Society of America Journal*, 68, 770–778.

Kelleners, T.J., & Verma, A.K. (2010). Measured and modeled dielectric properties of soils at 50 megahertz. *Soil Science Society of America Journal*, 74(3), 744 – 752.

Kizito, F., Campbell, C.S., Campbell, G.S., Cobos, D.R., Teare, B.L., Carter, B., & Hopmans, J.W. (2008) Frequency, electrical conductivity and temperature analysis of a low-cost capacitance soil moisture sensor. *Journal of Hydrology*, 352, 367–378.

Krogh, L., Madsen, H.B., & Greve, M.H. (2000). Cation exchange capacity pedotransfer functions for Danish soils. *Acta Agriculturae Scandinavica - Section B Soil and Plant Science*, 50, 1–12.

Lesch, S.M., Herrero, J., & Rhoades, J. (1998). Monitoring for temporal changes in soil salinity using electromagnetic induction techniques. *Soil Science Society of America Journal*, 62, 232–242.

Lesch, S.M., Rhoades, J.D., & Corwin, D.L. (2000). The ESAP-95 version 2.01R User Manual and Tutorial Guide. Research Report No. 146. Riverside (California): USDA-ARS, George E. Brown, Jr., Salinity Laboratory.

Lesch, S.M., Strauss, D.J., & Rhoades, J.D. (1995). Spatial prediction of soil salinity using electromagnetic induction techniques 1. Statistical prediction models: a comparison of multiple linear regression and cokriging. *Water Resources Research*, 31(2), 373–386.

McKenzie, R.C., Chomistek, W., & Clark, N.F. (1989). Conversion of electromagnetic inductance readings to saturated paste extract values in soils for different temperature, texture, and moisture conditions. *Canadian Journal of Soil Science*, 69(1), 25–32.

McNeill, J.D. (1980). Electromagnetic Terrain Conductivity Measurement at Low Induction Numbers. Tech. note TN-6. Ontario (Canada): Geonics Pty Ltd.

McNeill, J.D. (1992). Rapid, accurate mapping of soil salinity by electromagnetic ground conductivity meters. Advances in Measurement of Soil Physical Properties: Bringing Theory Into Practice, Spec. Pub., 30 (pp. 209–229). Madison (Wisconsin): Soil Science Society of America.

Nelson, D.W., & Sommers, L.E. (1996). Total carbon, organic carbon and organic matter. In: D.L. Sparks, A.L. Page, P.A. Helmke, R.H. Loeppert, P.N. Soltanpour, M.A. Tabatabai, C.T. Johnston & M.E. Sumner (Eds.), Methods of Soil Analysis Part 3—Chemical Methods (pp. 961–1010). Madison (Wisconsin): SSSA, ASA.

Ortiz, R., García, A.F., Sánchez, A., Marín, P., Delgado, M.J., Hernández, J., & Álvarez, J. (2008). Riesgos de Salinización y Alcalinización de la Red de Riegos del Bajo Segura. Murcia (Spain): Fundación Instituto Euromediterráneo del Agua.

Rallo, G., Provenzano, G., Castellini, M., & Sirera, A.P. (2018). Application of EMI and FDR sensors to assess the fraction of transpirable soil water over an olive grove. *Water*, 10(2), 168.

Reedy, R.C., & Scanlon, B.R. (2003). Soil water content monitoring using electromagnetic induction. *Journal of Geotechnical and Geoenvironmental Engineering*, 129(11), 1028–1039.

Rhoades, J.D. (1996). Salinity: electrical conductivity and total dissolved solids. In: D.L. Sparks, A.L. Page, P.A. Helmke, R.H. Loeppert, P.N. Soltanpour, M.A. Tabatabai, C.T. Johnston & M.E. Sumner (Eds.), Methods of Soil Analysis Part 3—Chemical Methods (pp. 417–435). Madison (Wisconsin): SSSA, ASA.

Rhoades, J.D., Chanduvi, F., & Lesch, S. (1999). Soil Salinity Assessment: Methods and Interpretations of Electrical Conductivity Measurements. FAO Irrigation and Drainage Paper 57. Rome: FAO.

Rhoades, J.D., Raats, P.A.C., & Prather, R.J. (1976). Effects of liquid-phase electrical-conductivity, water-content, and surface conductivity on bulk soil electrical-conductivity. *Soil Science Society of America Journal*, 40(5), 651–655.

Saey, T., Van Meirvenne, M., Vermeersch, H., Ameloot, N., & Cockx, L. (2009). A pedotransfer function to evaluate the soil profile textural heterogeneity using proximally sensed apparent electrical conductivity. *Geoderma*, 150 (3–4), 389–395.

Sheets, K.R., & Hendrickx, J.M.H. (1995). Noninvasive soil water content measurement using electromagnetic induction. *Water Resources Research*, 31(10), 2401–2409.

Sudduth, K.A., Drummond, S.T., & Kitchen, N.R. (2001). Accuracy issues in electromagnetic induction sensing of soil electrical conductivity for precision agriculture. *Computers and Electronics in Agriculture*, 31(3), 239–264.

Sudduth, K.A., Kitchen, N.R., Wiebold, W.J., Batchelor, W.D., Bollero, G.A., Bullock, D.G., Clay, D.E., Palm, H.L., Pierce, F.J., Schuler, R.T., & Thelen, K.D. (2005). Relating apparent electrical conductivity to soil properties across the north-central USA. *Computers and Electronics in Agriculture*, 46 (1–3 SPEC. ISS.), 263–283.

Taghizadeh-Mehrjardi, R., Minasny, B., Sarmadianc, F., & Malone, B.P. (2014). Digital mapping of soil salinity in Ardakan region, central Iran. *Geoderma*, 213, 15–28.

Triantafilis, J., Ahmed, M.F., & Odeh, I.O.A. (2002). Application of a mobile electromagnetic sensing system (MESS) to assess cause and management of soil salinization in an irrigated cotton-growing field. *Soil Use and Management*, 18, 330–339.

Triantafilis, J., Huckel, A.I., & Odeh, I.O.A. (2001). Comparison of statistical prediction methods for estimating field-scale clay content using different combinations of ancillary variables. *Soil Science*, 166(6), 415–427.

Triantafilis, J., Laslett, G.M., & McBratney, A.B. (2000). Calibrating an electromagnetic induction instrument to measure salinity in soil under irrigated cotton. *Soil Science Society of America Journal*, 64, 1000–1017.

Visconti, F. (2009). Elaboración de un Modelo Predictivo de la Acumulación de Sales en Suelos Agrícolas de Regadío bajo Clima Mediterráneo: Aplicación a la Vega Baja del Segura y Bajo Vinalopó (Alicante). PhD thesis. València (Spain): Universitat de València EG.

Visconti, F., Martínez, D., Molina, Mª J. Ingelmo, F., & de Paz, J.M. (2014). A combined equation to estimate the soil pore-water electrical conductivity: calibration with the WET and 5TE sensors. *Soil Research*, 52, 419–430.

Visconti, F., & de Paz, J.M. (2012). Prediction of the soil saturated paste extract salinity from extractable ions, cation exchange capacity, and anion exclusion. *Soil Research*, 50, 536–550.

Visconti, F., & de Paz, J.M. (2016). Electrical conductivity measurements in agriculture: the assessment of soil salinity. In: L. Cocco (Ed.), New Trends and Developments in Metrology (pp. 99–126). Rijeka (Croatia): Intech.

Visconti, F., & de Paz, J.M. (2018). Cómo conocer la salinidad del suelo mediante medidas de conductividad eléctrica. *Levante Agrícola: Revista Internacional de Cítricos*, 441, 98–103.

Visconti, F., & de Paz, J.M. (2020). Data accompanying the article titled "A semi-empirical model to predict the EM38 electromagnetic induction measurements of soils from basic ground properties" (see Data Availability statement).

Weller, U., Zipprich, M., Sommer, M., Zu Castell, W., & Wehrhan, M. (2007). Mapping clay content across boundaries at the landscape scale with electromagnetic induction. *Soil Science Society of America Journal*, 71(6), 1740–1747.

Yao, R., & Yang, J. (2010). Quantitative evaluation of soil salinity and its spatial distribution using electromagnetic induction method. *Agricultural Water Management*, 97(12), 1961–1970.

Zhdanov, M.S. (2018). Principles of ill-posed inverse problem solution. In: M. S. Zhdanov (Ed.), Foundations of Geophysical Electromagnetic Theory and Methods 2nd Ed. (pp. 269-287). Amsterdam: Elsevier.

Zhu, Q., Lin, H., & Doolittle, J. (2010). Repeated electromagnetic induction surveys for determining subsurface hydrologic dynamics in an agricultural landscape. *Soil Science Society of America Journal*, 74(5), 1750–1762.

TABLES

Table 1 Characteristics of some relevant electromagnetic induction studies using the EM38 and focusing on the detection of basic soil properties down to a maximum of 1.5 m depth.

Soil property	**Study area extension/ ha**	**Calibration (Sites × times)**	**Calibration R^2**	**Reference**
σ_e	2,066	12	0.86	Dakak et al. (2017)
σ_e	72,000	173	0.14 – 0.67	Taghizadeh-Mehrjardi et al. (2014)
σ_e	400	84	0.82 – 0.96	Yao and Yang (2010)
σ_e	21	6	0.80 – 0.86	Doolittle et al. (2001)
σ_e	0.94	62	0.80	Lesch et al. (1998)
σ_e	0.40 – 0.54	13 – 20	0.67 – 0.85	Díaz and Herrero (1992)
σ_e	12,000,000	694 – 796	0.63 – 0.85	McKenzie et al. (1989)
θ_w	0.60	200	0.87	Huang et al. (2018)
θ_w	13	47	0.86	Rallo et al. (2018)
θ_w	19.5	91	0.35 – 0.47	Zhu et al. (2010)
θ_w	0.01	113	0.58 – 0.85	Brevik et al. (2006)
θ_w	0.06	350	0.80 – 0.84	Reedy and Scanlon (2003)
θ_w	0.78	1040	0.58 – 0.64	Sheets and Hendrickx (1995)
θ_w	1.50	52	0.96	Kachanoski et al. (1988)
w_c	300,000	88	0.81	Saey et al. (2009)
w_c	14	46	0.66	Weller et al. (2007)
w_c	332	144 – 240	0.61	Sudduth et al. (2005)
w_c	12	24	0.65 – 0.72	Hedley et al. (2004)
w_c	244	46	0.72 – 0.77	Triantafilis et al. (2001)
w_{om}	10	80	0.36	García-Tomillo et al. (2017)
ρ_b	4	65	0.35	Jung et al. (2005)

Table 2 Parameters of the model represented by Eq. 15 that were obtained in previous works by simple linear regression.

Parameter	**σ_{p0}/ dS m^{-1}**	**k_σ**	**w_{e0}**	**$k_{c,e}$**	**CEC_0/ $mmol_C$ kg^{-1}**	**$k_{c,CEC}$/ $mmol_C$ kg^{-1}**	**$k_{om,CEC}$/ $mmol_C$ kg^{-1}**
Value	0.4 ± 0.4	0.71 ± 0.03	0.11 ± 0.03	0.96 ± 0.09	-12 ± 9	282 ± 24	2310 ± 320
Equation	6		7		9		
Reference	Visconti and de Paz, 2018		Visconti, 2009				

Table 3 Statistical summary of the Tikhonov regularization parameter (λ), average σ_b, skin depth (δ) and induction number (N_B) for each site in both surveys.

	First survey				Second survey			
	λ	**σ_b/ dS m^{-1}**	**δ/m**	**N_B**	**λ**	**σ_b/ dS m^{-1}**	**δ/m**	**N_B**
Count	28	28	28	28	28	28	28	28
Mean	0.446	0.674	19.0	0.059	0.435	0.852	16.9	0.067
Std. Dev.	0.086	0.419	6.9	0.020	0.100	0.496	7.2	0.021
Max.	0.752	1.76	35.1	0.100	0.689	2.50	41.5	0.120
Min.	0.339	0.14	9.9	0.029	0.300	0.10	8.3	0.024
Skewness	0.69	-0.26	1.45	-0.72	1.01	0.13	0.99	-0.31

Table 4 Coefficient of determination (R^2) and root mean square error (RMSE) in units of dS m^{-1} and in percentage of the model for σ_b* prediction in both dipole mode orientations for all measurements and separately for each height in the calibration, cross-validation and external validation data analyses.

Data analysis	**Height/ cm**	**R^2**		**RMSE/dS m^{-1}**		**RMSE (%)**	
		Vertical	**Horizontal**	**Vertical**	**Horizontal**	**Vertical**	**Horizontal**
Calibration	0	0.749	0.763	0.346	0.218	37.9	27.6
Calibration	50	0.787	0.786	0.141	0.092	28.1	36.6
Calibration	100	0.788	0.770	0.097	0.046	28.5	27.4
Calibration	150	0.720	0.726	0.082	0.038	32.7	31.1
Calibration	200	0.720	0.727	0.054	0.027	31.2	30.6
Calibration	All	0.839	0.895	0.178	0.110	40.8	38.7
Cross-validation	0	0.690	0.708	0.360	0.242	39.5	30.6
Cross-validation	50	0.730	0.727	0.163	0.107	32.3	42.4
Cross-validation	100	0.736	0.714	0.107	0.053	31.3	32.2
Cross-validation	150	0.656	0.664	0.090	0.042	35.9	35.0
Cross-validation	200	0.657	0.664	0.062	0.031	35.6	35.0
Cross-validation	All	0.801	0.870	0.189	0.123	43.4	43.3
External validation	0	0.647	0.796	0.502	0.215	45.2	26.3
External validation	50	0.699	0.757	0.262	0.120	37.2	30.1
External validation	100	0.700	0.695	0.182	0.081	39.0	36.2
External validation	150	0.693	0.659	0.089	0.081	32.3	33.9
External validation	200	0.659	0.621	0.066	0.035	33.2	35.4
External validation	All	0.793	0.894	0.271	0.119	49.1	35.5

FIGURE CAPTIONS

Figure 1 Study area and placement of the sites visited in the first and second survey.

Figure 2 Monthly rainfall and FAO's reference evapotranspiration (ET_0) in the study area in 2006 (1st survey) and 2010 (2nd survey)

Figure 3 Flowchart of the calibration and validation of the semi-empirical model

Figure 4 Measurements of σ_b* in the vertical and the horizontal dipole modes and in the first and the second soil surveys.

Figure 5 Calculated σ_b at the different soil depths for all the sites visited in the first and the second surveys.

Figure 6 Predicted (σ_b') against WET-2-measured (σ_b) soil bulk electrical conductivity on the basis of the 1D inversion done with the data of the first survey (a) and on the basis of the application of Eq. 15 to the data of the second survey (b).

Figure 7 Predicted (σ_b*') against observed (σ_b*) values of soil depth-weighted electrical conductivity as measured with the EM38 in the horizontal coplanar (H) and vertical coplanar (V) dipole modes in the calibration, cross-validation and external validation.

Figure 1.

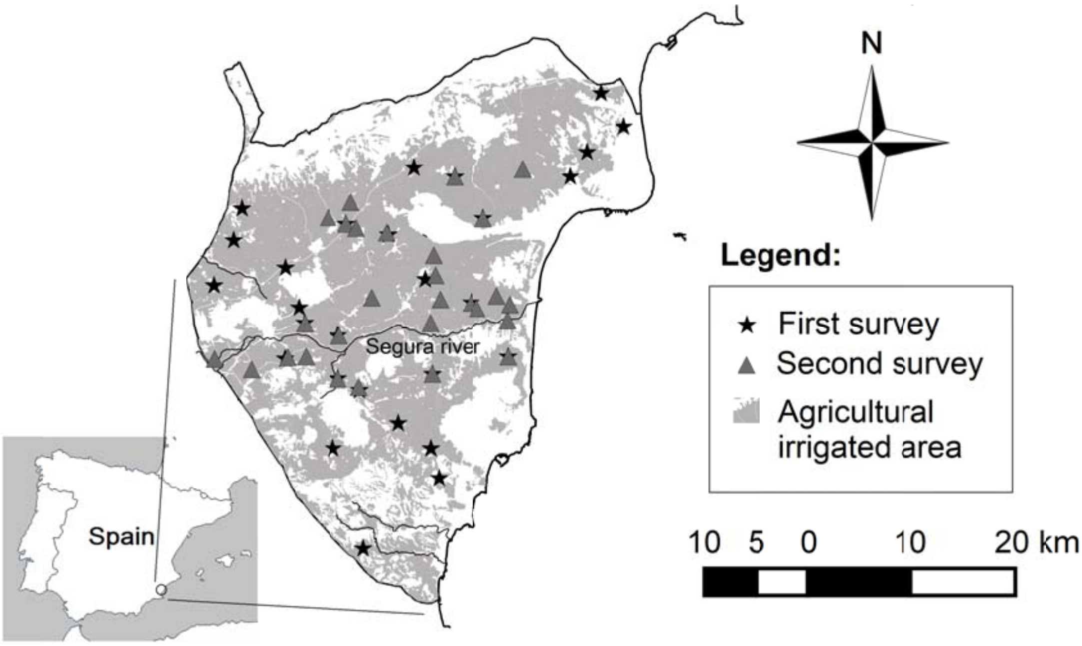
N
Legend:
First survey
Second survey
Agricultural irrigated area
10 5 0 10 20 km
Segura river
Spain

Figure 2.

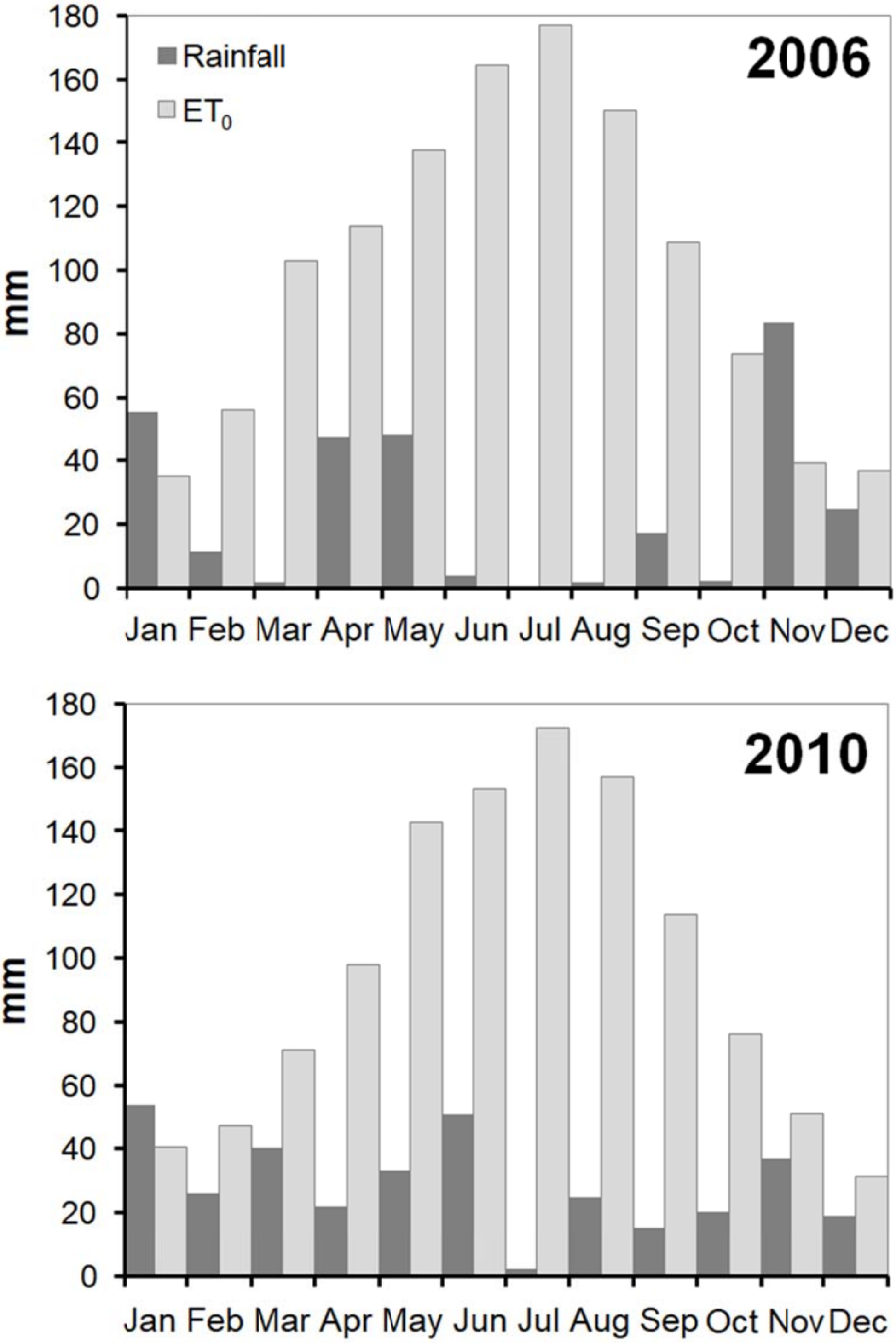
2006
Rainfall
ET0
mm
180
160
140
120
100
80
60
40
20
0
Jan Feb Mar Apr May Jun Jul Aug Sep Oct Nov Dec
2010
mm
180
160
140
120
100
80
60
40
20
0
Jan Feb Mar Apr May Jun Jul Aug Sep Oct Nov Dec

Figure 3.

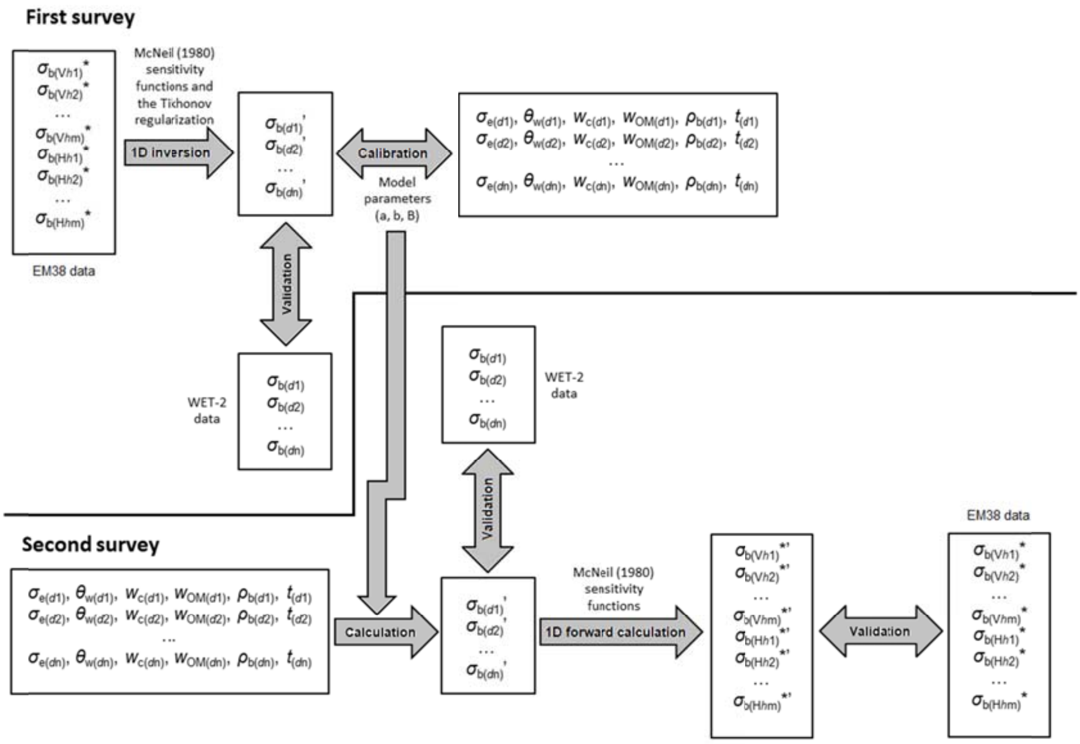

First survey
McNeil (1980) sensitivity functions and the Tichonov regularization
1D inversion
Calibration
Model parameters (a, b, B)
EM38 data
Validation
WET-2 data
WET-2 data
Validation
Second survey
Calculation
McNeil (1980) sensitivity functions
1D forward calculation
Validation
EM38 data

Figure 4.

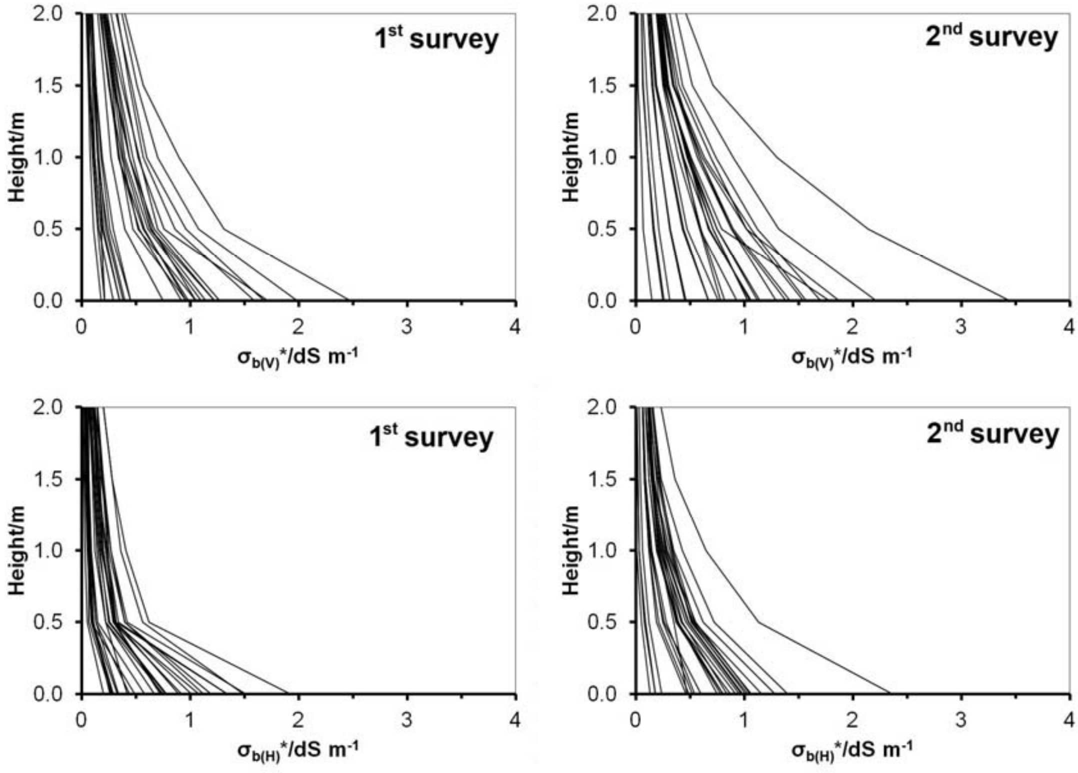
1st survey
2nd survey
1st survey
2nd survey
Height/m
2.0
1.5
1.0
0.5
0.0
0
1
2
3
4
σb(V)*/dS m-1
σb(H)*/dS m-1

Figure 5.

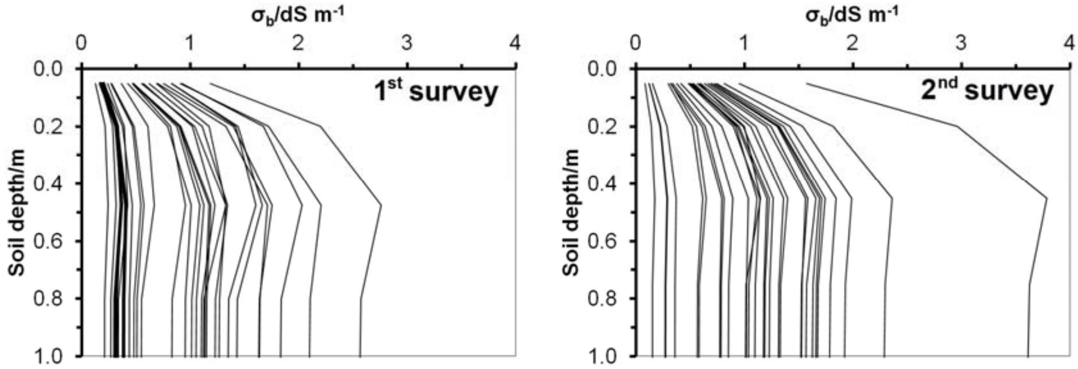
σb/dS m-1
0
1
2
3
4
0.0
0.2
0.4
0.6
0.8
1.0
Soil depth/m
1st survey
2nd survey

Figure 6.

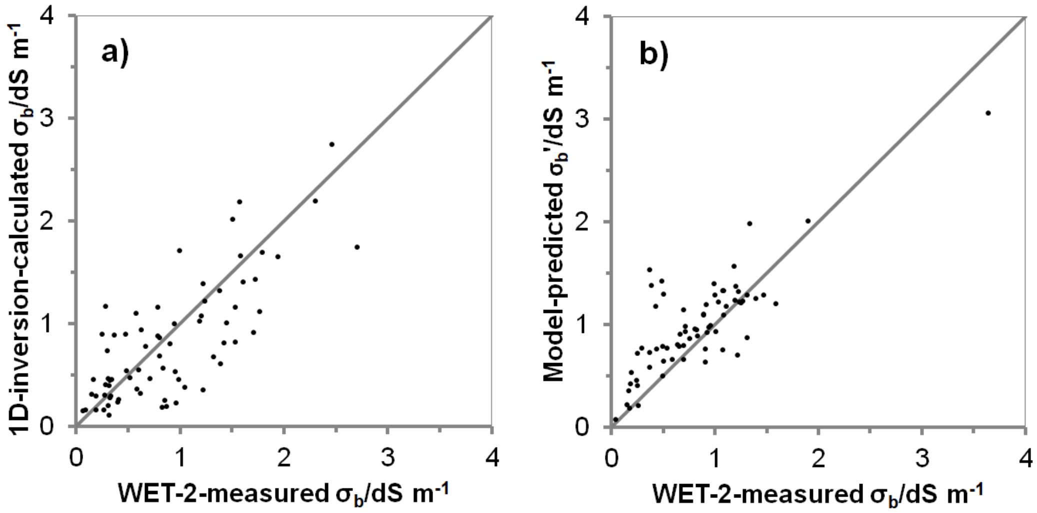
a)
1D-inversion-calculated σb/dS m-1
WET-2-measured σb/dS m-1
b)
Model-predicted σb'/dS m-1
WET-2-measured σb/dS m-1
0
1
2
3
4

Figure 7.

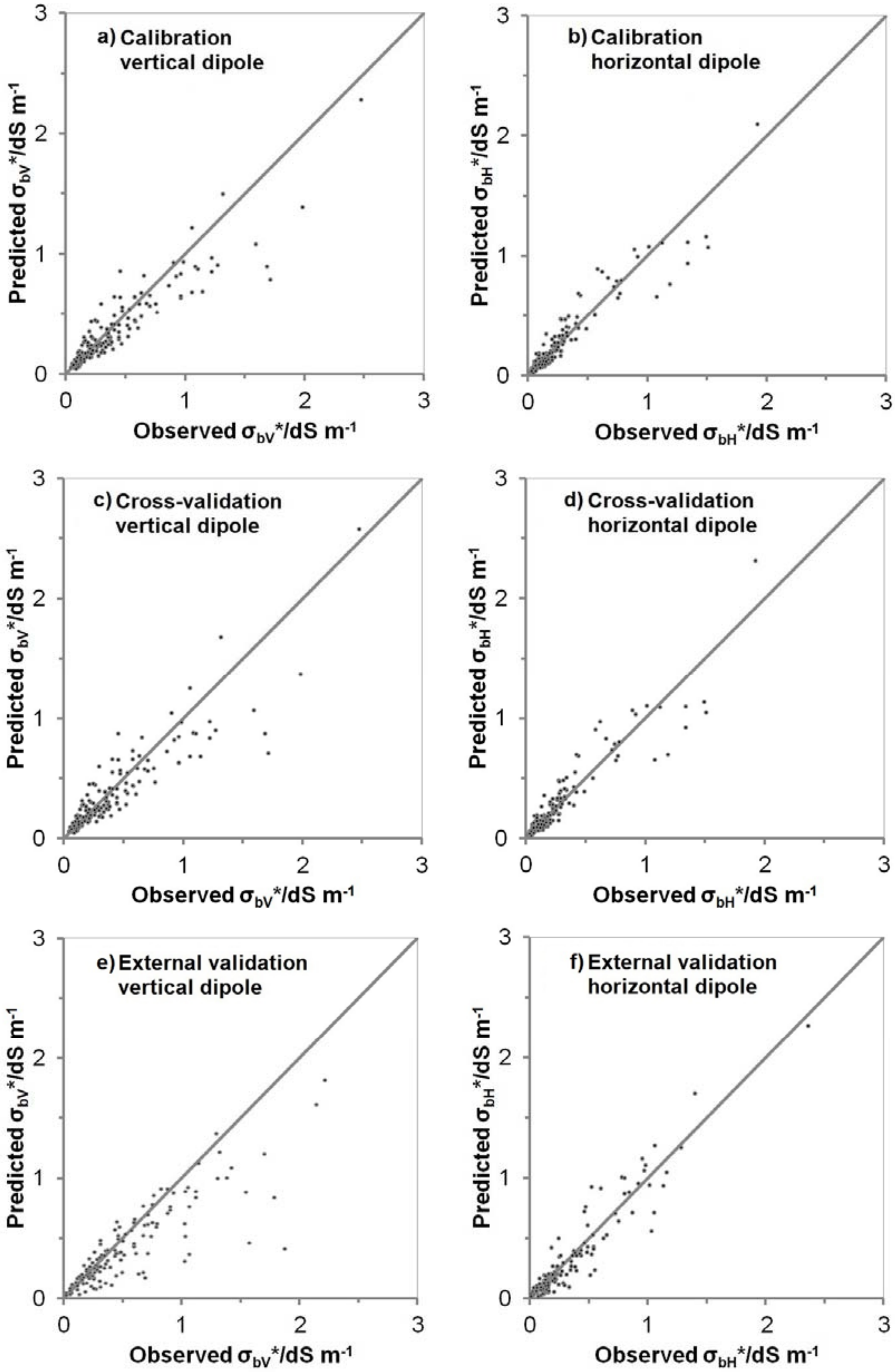
a) Calibration vertical dipole
b) Calibration horizontal dipole
c) Cross-validation vertical dipole
d) Cross-validation horizontal dipole
e) External validation vertical dipole
f) External validation horizontal dipole
Predicted σbV*/dS m-1
Observed σbV*/dS m-1
Predicted σbH*/dS m-1
Observed σbH*/dS m-1
0
1
2
3